Application of swirl and spin for in-flight thrust modulation of hybrid rocket engines

Markus Bockelt and David Greatrix***
**Munich University of Applied Sciences*
Loth Strasse 34, Munich, Germany
***Ryerson University*
350 Victoria Street, Toronto, Ontario, Canada

Abstract
Alternative approaches for controlling the thrust level of an N_2O/HTPB hybrid rocket engine (HRE) over the course of a rocket vehicle's flight mission are examined in this computational study. One on-command approach for modulating the thrust of an HRE is based on applying different levels of swirl to the incoming head-end oxidizer flow, which in turn delivers the required fuel burning rate increase and corresponding thrust level. The other on-command approach that is looked at for modulating the thrust of an HRE is based on spinning the engine about the engine's longitudinal axis at a given rate to deliver the required thrust level.

1. Introduction

In terms of flight management flexibility and capability, the performance of rocket vehicles can benefit from the on-command raising or lowering of the vehicle's in-flight thrust delivery. The wider the on-command thrust range capability, the greater the mission flexibility. In the case of hybrid rocket engines (HREs), one has the inherent ability to throttle the oxidizer mass flow delivery to the combustion chamber, thus giving some thrust modulation capability, even for simple axial head-end oxidizer injection configurations. However, the effective range for thrust modulation may not be sufficient for some flight missions, using the standard axial injection setup.

In the present computational study, alternative techniques for providing significant thrust modulation capability for hybrid rocket propulsion systems are investigated. The application of oxidizer swirl will be considered (a tangential shear flow component above the burning fuel surface results in a heightened fuel surface regression rate, which ultimately translates into a higher thrust delivery). As a second alternative approach, the application of engine spin will be considered (spin produces a normal acceleration field that acts to compress the flame zone above the burning fuel surface, which in turn potentially results in significant burning rate augmentation, which ultimately can translate into a higher thrust delivery).

A reference flight vehicle will be used as the basis for providing some sample performance results for the two thrust modulation techniques applied to a baseline HRE, and allow for some comparisons between the two setups (see Fig. 1). The flight vehicle, representative of a small single-stage sounding rocket, has a body diameter of around 6 inches (15.24 cm) and an overall vehicle length of around 2.2 m, thus allowing for a propulsion system length of around 1.55 m.

2. Hybrid rocket engine under swirl

A conventional propellant combination is employed for the reference HRE, with nitrous oxide (N_2O) as the liquid oxidizer and hydroxyl-terminated polybutadiene (HTPB) as the solid fuel. As a positive in terms of specific impulse I_{sp}, the flame temperature T_F is relatively high, being around 2800 K. The nominal stoichiometric oxidizer-to-fuel mixture ratio for the two propellants is around 6.5, with the corresponding vehicle loading being comparable (16.4 kg of N_2O, 2.6 kg of HTPB). A cylindrical-grain configuration is chosen, being most amenable to burning-rate augmentation under a head-end injection swirling flow. A single port setup is also preferable to a multiple-port configuration, in general [1], as long as there is a sufficient burning surface area for the corresponding fuel regression rate. Note that slower-burning HREs may need to use a multiple-port setup above a threshold engine size (burning

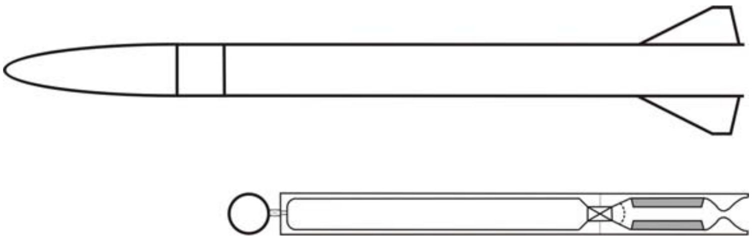

Figure 1: Schematic diagram of the reference flight vehicle (top), with the baseline HRE propulsion system (bottom) shown underneath

rate tending to decrease, as port diameter increases). Under baseline no-swirl conditions, the cylindrical grain design used here will produce a relatively neutral (constant) thrust-time profile for most of the main (quasi-steady) firing phase.

2.1 Computational modelling

In this internal ballistic study involving swirl, the solid fuel surface regression rate will be a function of the flow (mass flux G) in the axial and tangential (swirl) directions. Referring to [2], the overall fuel regression rate r_b can be estimated via:

$$r_b = \frac{(h_x^* + h_\theta^*)}{\rho_s C_p} \ell n[1 + \frac{C_p}{C_s} \frac{(T_f - T_s)}{(T_s - T_i - \Delta H_s / C_s)}] \quad \textbf{(1)}$$

The logarithmic relation above arises from a thin-film-theory treatment of the transpiration effect on the convective heat transfer to the burning fuel surface. The parameters h_x* and h_θ* are the zero-transpiration convective heat transfer coefficient for the axial and tangential directions, respectively. These variables, a function of axial and tangential mass flux G_x and G_θ, may be determined from Reynolds' analogy, here assuming turbulent flow, so that:

$$h_x^* = \frac{k^{2/3} {C_p}^{1/3}}{\mu^{2/3}} \frac{G_x f_x^*}{8} \quad \textbf{(2)}$$

and

$$h_\theta^* = \frac{k^{2/3} {C_p}^{1/3}}{\mu^{2/3}} \frac{G_\theta f_\theta^*}{8} \quad \textbf{(3)}$$

The parameter f* is the respective zero-transpiration Darcy-Weisbach friction factor for each direction, which may be estimated via Colebrook's well-known equation [1], which includes fuel surface roughness height ε:

$$(f_x^*)^{-1/2} = -2\log_{10}[\frac{2.51}{Re_d (f_x^*)^{1/2}} + \frac{\varepsilon / d}{3.7}] \quad \textbf{(4)}$$

and

$$(f_\theta^*)^{-1/2} = -2\log_{10}[\frac{2.51}{Re_{d,\theta} (f_\theta^*)^{1/2}} + \frac{\varepsilon / d_\theta}{3.7}] \quad \textbf{(5)}$$

The effective hydraulic diameter in the tangential direction, d_θ, which in turn is used for the effective tangential-flow Reynolds number $Re_{d,\theta}$, can be found via

$$d_\theta = \frac{4A_\theta}{P_\theta} \approx 4\delta \tag{6}$$

where A_θ is the effective flow cross-sectional area for the near-surface tangential flow (this flow being at a peak velocity V, and of boundary layer thickness δ) and P_θ is the effective peripheral distance around that rectangular cross-sectional area (assuming a simple cylindrical fuel grain shape). The parameter δ can alternatively be defined as the effective separation distance between the oxidizer injection port centre-line radial location and the current fuel grain surface radial location.

One can refer to Fig. 2 for sample curves illustrating the burning (regression) rate r_b of the study's solid fuel as a function of axial mass flux, at three different swirl numbers (S). With respect to swirl number, one can note the following relationship between S and swirl angle ψ, where U is the nominal peak axial velocity and V is the peak tangential velocity:

$$S = \frac{\int_0^{r_o} r^2 v_\theta u_x \mathrm{d}r}{r_o \int_0^{r_o} r[u_x^2 + (\frac{p - p_\infty}{\rho})]\mathrm{d}r} \approx \frac{2}{3}\tan\psi \approx \frac{2}{3}\frac{V}{U} \tag{7}$$

The curve calculations are based on a mid-firing port diameter d (around 8 cm), and corresponding tangential injection separation distance δ (around 2.5 cm) at that point into the firing simulation.

At a given time into a simulated HRE firing, a straightforward quasi-steady finite-difference solution [1] can be obtained for the one-dimensional (x-dependent) flow and fuel regression-rate values moving (from the engine's combustor head end) downstream to the end (port) of the fuel grain; further downstream, one can compute the aft gas flow (or gas-particle, if a two-phase medium) through and out of the engine's exhaust nozzle. Repeating these calculations for each time step of the simulated HRE firing, one can ultimately produce a combustor head-end pressure-time profile for the overall firing, which in turn allows one to produce a corresponding thrust-time profile. Stoichiometric length (the nominal point downstream of the combustion chamber's head end where the oxidizer is completely consumed) can also be tracked with time into the simulated firing.

In the present simulation program, the use of the fully reacted gas properties (e.g., molecular mass of 26 amu, ratio of specific heats of 1.2) is maintained throughout the central port flow domain, regardless of the stoichiometric length L_{st} . This may result in some over-prediction of thrust delivery (and I_{sp}) when L_{st} is substantially above or below the fuel grain length L_f. For example, N_2O decomposes exothermically into N_2 (molecular mass of 28 amu) and O_2 (molecular mass of 32 amu) when temperatures are greater than around 850 K; for L_{st} substantially greater than L_f , one might expect the mean core flow gas molecular mass to be higher than 26 amu, hence acting to reduce the expected thrust delivery.

2.2 Numerical results for swirling HRE

A simple duty cycle for swirling the vehicle's HRE injected oxidizer flow at a selected time into a simulated firing will be demonstrated first for a moderate swirl number of 2. The means by which one might in practice implement the swirling will be discussed a bit later in the paper. Referring to the combustor head-end pressure-time profile of Fig. 3, the swirling, and augmented oxidizer mass flow, is commenced at 3 s into the simulated firing. A modest step increase in chamber pressure is observed. The reduction of the pressure level with time during the swirl period is due to grain burnback, which increases δ and thus d_θ, which acts to reduce the swirl-driven component of the fuel regression rate. The upstream injection feed pressure would need to be higher than the combustion chamber pressure at all times during the firing. Forward acceleration of the rocket vehicle is not an influencing factor on the burning process, for these HRE firings. The simulated firing ends when the loaded oxidizer is completely depleted.

One can observe the corresponding sea-level thrust-time profile in Fig. 4. The average specific impulse for the nominal (no-swirl) firing is around 217 s, and just slightly higher for the swirl case. The total impulse for the nominal firing is not overly impressive at around 37000 N·s, largely as a result of the lower mean chamber pressure in the case of the HRE's overall firing. That being said, the more prolonged, but lower, thrust delivery may be advantageous for sustained thrust delivery flight mission segments (versus short-term boost-phase mission segments, say for initial launch and ascent, where high thrust is advantageous).

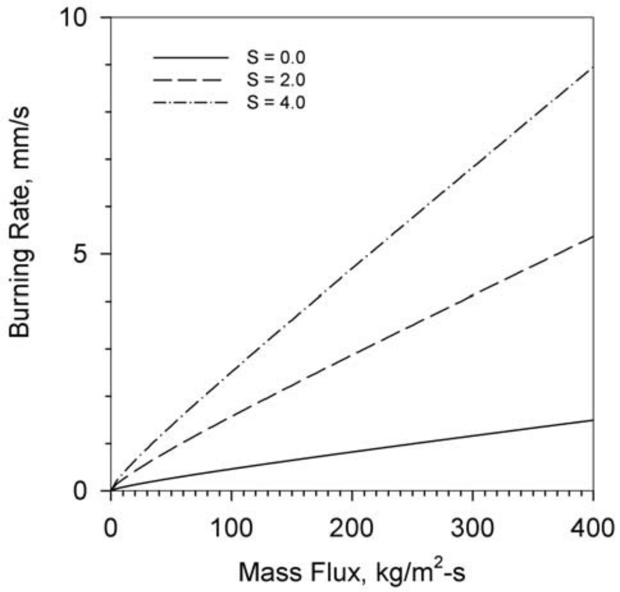

Figure 2: Fuel surface regression rate of N_2O/HTPB propellant combination as function of axial mass flux, at three different swirl numbers (mid-firing geometric reference)

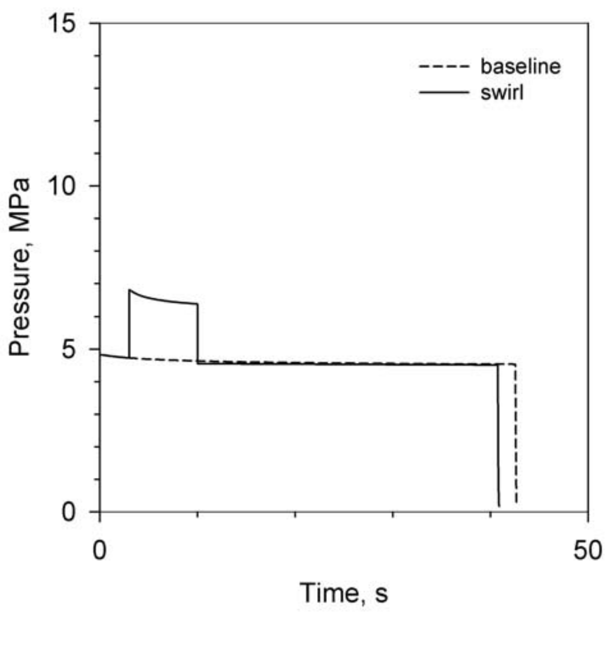

Figure 3: Combustor head-end pressure-time profiles of N_2O/HTPB hybrid rocket engine, baseline case (oxidizer mass flow of 0.385 kg/s), and manoeuvring case with swirl (S = 2) and augmented oxidizer mass flow (0.485 kg/s), 3 s < t < 10 s

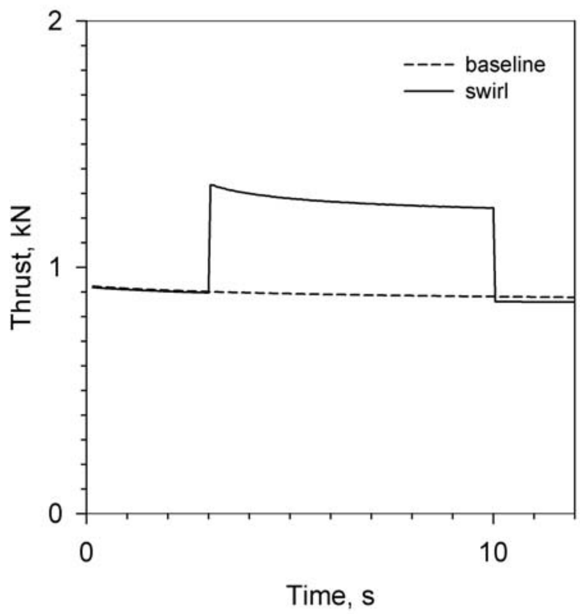

Figure 4: Early part of sea-level thrust-time profiles of N_2O/HTPB hybrid rocket engine, baseline case (oxidizer mass flow of 0.385 kg/s), and manoeuvring case with swirl (S = 2) and augmented oxidizer mass flow (0.485 kg/s), 3 s < t < 10 s

The corresponding stoichiometric length profiles with respect to the HRE's firing time can be found in Fig. 5. The length L_{st} is given in terms of percentage of the actual fuel grain length (which is 24 cm); when greater than 100%, the estimate is based on an imaginary extension of the fuel port further downstream. One can see that the nominal no-swirl operating condition results in unreacted oxidizer remaining upon nozzle entry (L_{st} > 100%). With the introduction of swirl, the heightened fuel regression rate brings down L_{st} quite a significant amount, to well below 100% (hence, no unreacted oxidizer remaining after the L_{st} position, leaving only non-combustive ablation, likely at a lower rate, of the fuel surface further downstream [1], with admission of a lower-temperature gas acting to cool the central flow). By increasing the incoming oxidizer mass flow to some degree during the swirl period, from 0.385 to 0.485 kg/s, it helps to keep the value of L_{st} from getting too low, and bring L_{st} back up to being closer to the ideal design case of 100%. Once the swirl is ended at 10 s (and the oxidizer mass flow is returned to 0.385 kg/s), the fuel grain's port is more expanded coming out of the swirl period, hence one observes a post-swirl L_{st} that's significantly higher than the baseline case, and thus, even further from the ideal 100% case.

A second duty cycle, with a higher swirl level (S = 4) and augmented oxidizer flow (0.975 kg/s), will now be evaluated. The combustor head-end pressure-time profile for this case is illustrated in Fig. 6. A more substantial increase in pressure is observed during the swirl period, relative to the previous case. As noted earlier, if running the engine for a period of time at such a high chamber pressure (close to 15 MPa), one would need to ensure that the oxidizer feed delivery pressure was adjusted upward to be some margin (say at least 20%) above the combustion chamber's pressure [1], for positive throughput and feed stability. The overall firing time of the HRE is shortened from 42 to 32 s, as a result of expending more oxidizer earlier on in the firing (about 0.5 kg of fuel remains unexpended at the end of this 32-s firing, while 1.55 kg is unused in the nominal 42-s baseline case).

The corresponding sea-level thrust-time profile for this case may be viewed in Fig. 7. One can observe the thrust delivery being tripled from its baseline level, as a result of the combined swirl and oxidizer flow input. The average specific impulse for this simulated firing is around 223 s, a small but noticeable increase over the previous case.

The corresponding stoichiometric length profiles may be found in Fig. 8. A considerable increase in the oxidizer mass flow is necessitated to keep the stoichiometric length from falling too low during the swirl period.

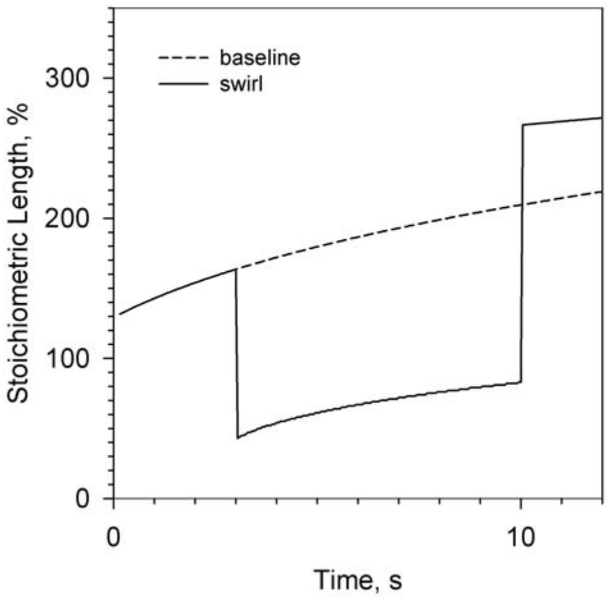

Figure 5: Early part of stoichiometric length-time profiles of N_2O/HTPB hybrid rocket engine, baseline case (oxidizer mass flow of 0.385 kg/s), and manoeuvring case with swirl (S = 2) and augmented oxidizer mass flow (0.485 kg/s), 3 s < t < 10 s

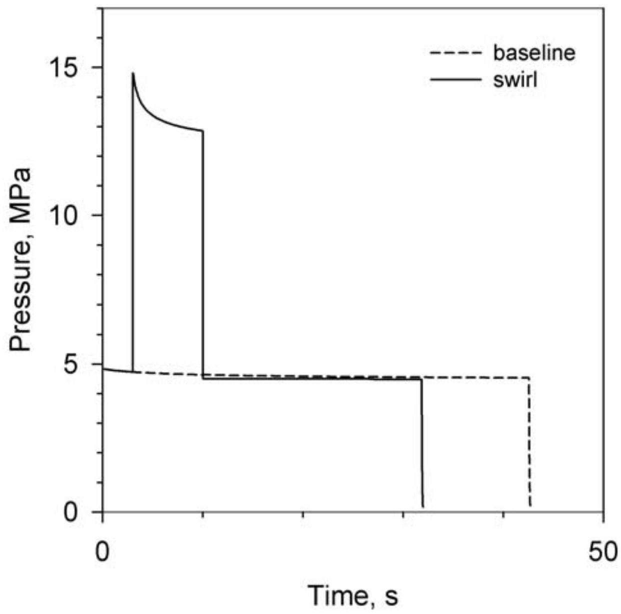

Figure 6: Head-end pressure-time profiles of N_2O/HTPB hybrid rocket engine, baseline case (oxidizer mass flow of 0.385 kg/s), and manoeuvring case with swirl (S = 4) and augmented oxidizer mass flow (0.975 kg/s), 3 s < t < 10 s

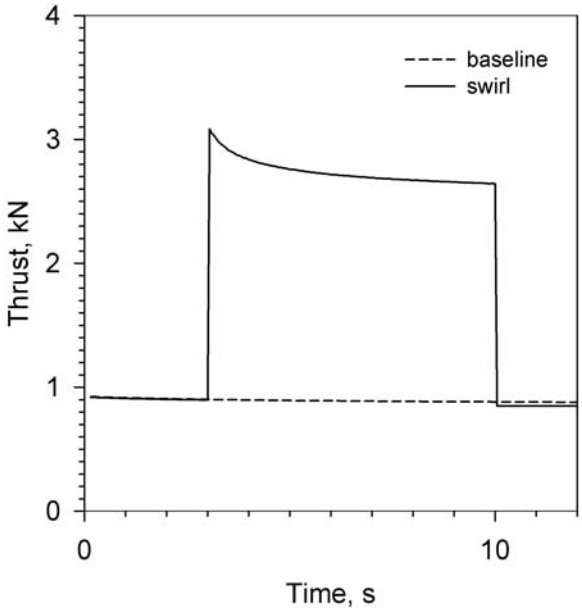

Figure 7: Early part of sea-level thrust-time profiles of N_2O/HTPB hybrid rocket engine, baseline case (oxidizer mass flow of 0.385 kg/s), and manoeuvring case with swirl (S = 4) and augmented oxidizer mass flow (0.975 kg/s), 3 s < t < 10 s

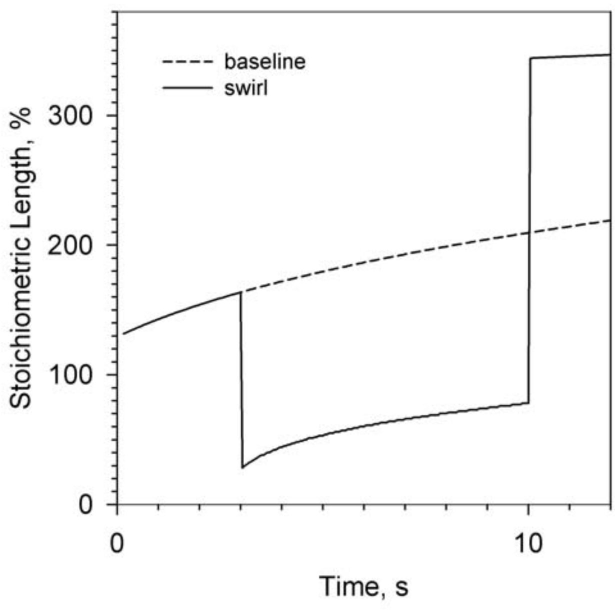

Figure 8: Early part of stoichiometric length-time profiles of N_2O/HTPB hybrid rocket engine, baseline case (oxidizer mass flow of 0.385 kg/s), and manoeuvring case with swirl (S = 4) and augmented oxidizer mass flow (0.975 kg/s), 3 s < t < 10 s

2.3 Possible approaches for HRE swirling

A number of different approaches have been used in HREs for swirling oxidizer flows from the engine's head end [2], the basis for the present study. For flight mission flexibility, one would want the ability to adjust the swirl, on command, to different levels, in a relatively expeditious manner. Additionally, as noted earlier, if one is making significant adjustments in chamber pressure while modulating the vehicle's thrust delivery, one needs to ensure the feed system pressure is adjusted accordingly, to avoid backflow, etc.

One example setup for applying different levels of swirl from a head-end injection system is illustrated in Fig. 9. Drawing from the liquid oxidizer storage tank upstream, a quick-response flow regulator provides the needed mass flow at the desired pressure to the different injection ports (main axial port(s), tangential ports) positioned downstream, as commanded by the on-board flight management computer. The pressure drop through the respective injector determines the resulting net flow velocity exiting the injector [1].

3. Hybrid rocket engine under spin

One should note that a considerable amount of experimental spin testing has shown that burning rates of aluminized and non-aluminized solid rocket motor (SRM) propellants (although not all, depending sometimes on the use of additives) can be quite sensitive to a normal acceleration field, generally moreso when the base burning rate is lower [1,3]. There has been no comparable testing reported for hybrid rocket engine fuels, as to their sensitivity in this regard. Bearing that in mind, some combustion behaviour is demonstrably similar between SRMs and HREs, e.g., axial mass flux-dependent burning behaviour [1]. For the remainder of this discussion, it will be presumed that a correlation of normal acceleration (induced by spin) and heightened fuel surface regression rates is a plausible phenomenon.

The same cylindrical-grain configuration and chemical combination used above for swirl is potentially amenable to burning-rate augmentation under a normal acceleration field (i.e., as produced from engine spin). The base burning rate is quite low, in enhancing the fuel's sensitivity to a_n .

3.1 Computational modelling

In this internal ballistic study of spin-induced a_n , the solid propellant burning rate will be a function of core flow (axial mass flux G) and acceleration. Modelling of core-flow (convective heat transfer) dependent burning in the presence of another mechanism (in this case, a_n , that provides a base burning rate contribution r_o) requires a modification to the calculation approach covered earlier for swirl. For overall burning rate, one now has :

$$r_b = r_o + r_G = r_o + \frac{h(T_F - T_S)}{\rho_s [C_s (T_S - T_i) - \Delta H_s]} \qquad \textbf{(8)}$$

where in the absence of swirl, convective heat transfer coefficient h (under transpiration) is based on the axial flow and base burning rate contributions. Here, one would also need the equation for h as a function of zero-transpiration h^* and overall regression rate r_b [1]:

$$h = \frac{\rho_s r_b C_p}{\exp(\frac{\rho_s r_b C_p}{h^*}) - 1} \qquad \textbf{(9)}$$

Moving to the second contribution by a_n , the roles are reversed, whereby the axial flow dependent contribution is treated now as the base rate r_o . From SRM analysis, based on the representation of the combustion zone as being compressed under an acceleration field, the principal equation of the acceleration-dependent burning-rate model is [1]:

$$r_b = [\frac{C_p (T_F - T_S)}{C_s (T_S - T_i) - \Delta H_s}] \frac{(r_b + G_a / \rho_s)}{exp[C_p \delta_o (\rho_s r_b + G_a) / k] - 1} \qquad \textbf{(10)}$$

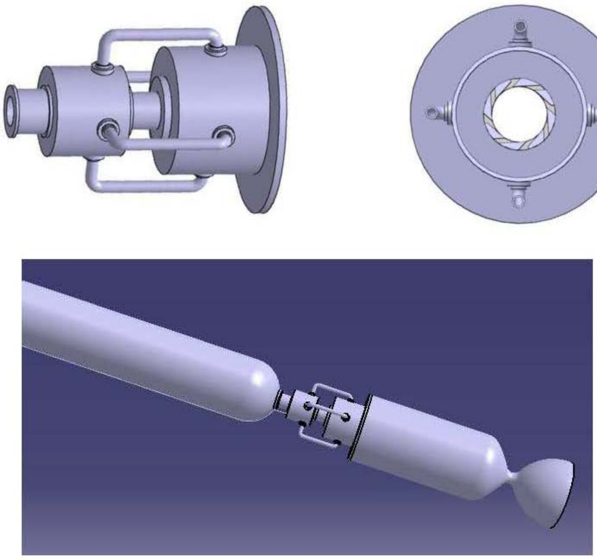

Figure 9: Illustration of head-end swirl approach, to provide adjustments in oxidizer mass flow and swirl level, upon command. Upper left image shows injection apparatus for regulated axial and tangential oxidizer flow input (axial flow moving left to right). Upper right image is the aft part of the injection apparatus, with an internal view of the tangential injection arrangement, looking rearward. Lower image shows rear portion of internal engine components, from oxidizer tank at left of diagram, to exhaust nozzle at right of diagram

The reference combustion zone thickness can be estimated via:

$$\delta_o = \frac{k}{\rho_s r_o C_p} \cdot \ell n[1 + \frac{C_p(T_F - T_S)}{C_s(T_S - T_i) - \Delta H_s}] \quad \textbf{(11)}$$

In the above, as noted, r_o is the base burning rate due to factors other than acceleration, e.g., due to core flow. The accelerative mass flux G_a, negative when a_n is directed into the combustion zone (i.e., compressing said zone) and zero when directed away from the surface, is determined from

$$G_a = \frac{a_n p}{r_b} \frac{\delta_o}{RT_F} \frac{r_o}{r_b} \cdot cos^2 \phi_d \quad \textbf{(12)}$$

This formula for G_a is more generally applicable than that stipulated in [1], in that it allows for r_o to vary in a given internal ballistic situation. The value for G_a is reduced by increasing values of the total lateral/longitudinal displacement angle (a.k.a., augmented orientation angle) ϕ_d:

$$\phi_d = tan^{-1}[K(\frac{r_o}{r_b})^3 tan\phi] \quad \textbf{(13)}$$

where the resultant acceleration (orientation) angle ϕ is defined by:

$$\phi = tan^{-1}(\frac{a_\ell}{a_n}) \tag{14}$$

The longitudinal or combined lateral/longitudinal acceleration component is given by a_ℓ. The correction factor K is set as 12 using Eq. (13), to be consistent with the results produced by the original equation for G_a, where the value for K was 8 [1].

One can refer to Fig. 10 for sample curves illustrating the overall burning rate r_b and the base burning rate r_o of the study's fuel as a function of a_n, at a nominal reference engine condition (low reference base burning rate of 0.62 mm/s at an axial mass flux of 125 kg/s·m^2). The reference base burning rate is markedly lower than a typical SRM base rate of the order of 10 mm/s, so the sensitivity to a_n here is markedly higher than what one would observe for an SRM [1]. As the value for r_b increases, the value for r_o progressively decreases. Moving to Fig. 11, one can observe the influence of a_ℓ in reducing the augmentation as ϕ gets bigger, via Eqs. (13) and (14). The lowermost predicted curve, for a_n = 0.05 g, is qualitatively similar in shape to those observed experimentally for SRM propellants at much higher values for a_n. The higher curves on the graph of Fig. 11 clearly become more rectangular, with the steep drop-off point shifting to the right (higher ϕ) as a_n gets larger in value. This predicted rectangularization and shifting also occurs for SRMs, but at much higher values for a_n.

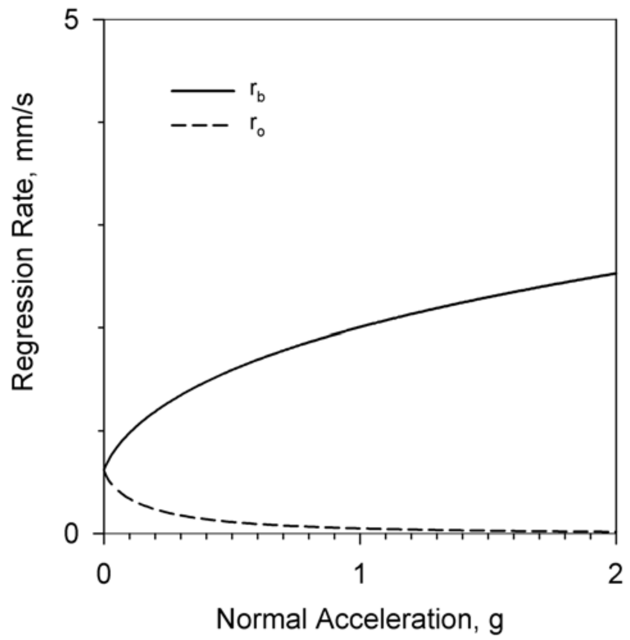

Figure 10: Burning rate and base rate of N_2O/HTPB propellant as function of normal acceleration, for $r_{o,ref}$ = 0.62 mm/s, G = 125 kg/s·m^2 and port diameter d_p = 0.05 m

3.2 Numerical results for spinning HRE

A simple duty cycle for spinning the vehicle's HRE at a selected point into a simulated firing will be demonstrated under static test conditions, e.g., as if the engine were being spun up on a test stand in the laboratory, so that longitudinal acceleration a_ℓ due to forward flight is not a factor on the combustion process. The means by which one might in practice implement the spinning will be discussed a bit later. Referring to the combustor head-end pressure-time profile of Fig. 12, the spinning is commenced at 3 s into the simulated firing. The mean level of normal acceleration felt at the burning propellant surface at 7 revolutions per second (rps) is around 10 g (note: as the propellant grain burns back, the radial position of the burning surface increases, hence a_n does increase in value with time while holding a constant engine rotation rate). The resulting progressive normal acceleration produces a progressive chamber pressure rise approaching 150% above the nominal no-spin chamber pressure value.

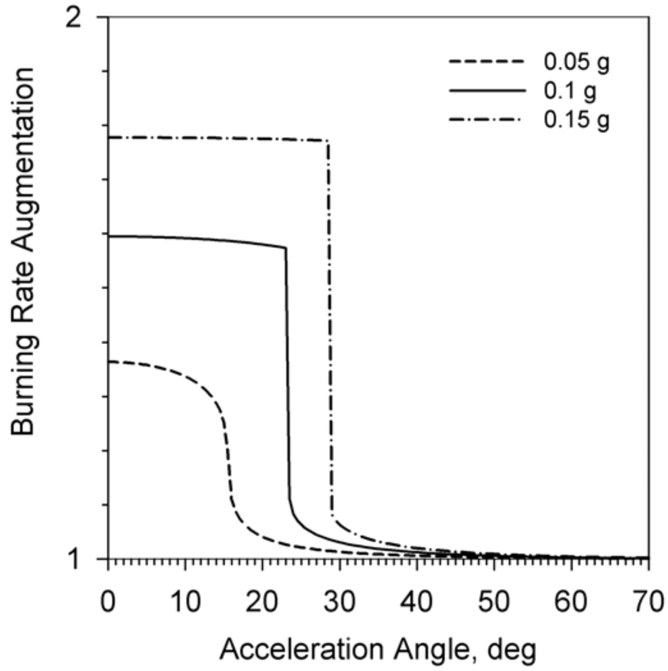

Figure 11: Burning rate augmentation of N_2O/HTPB propellant as function of resultant acceleration angle ϕ, at three different a_n levels

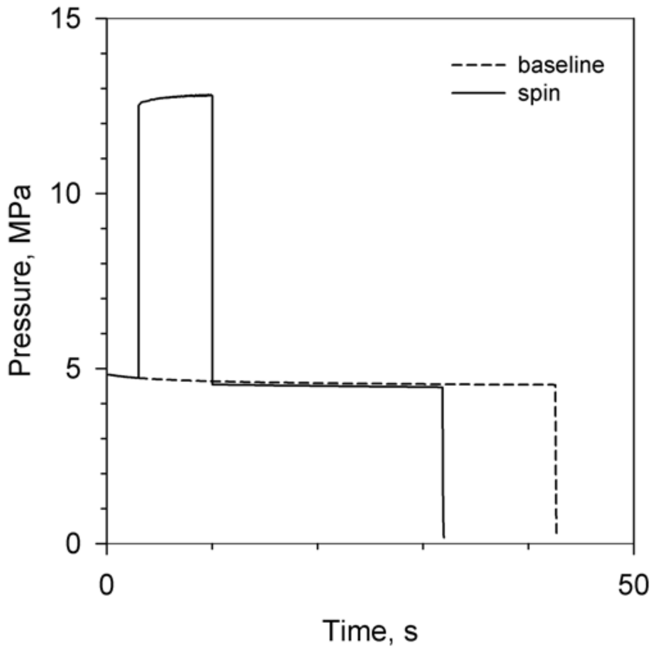

Figure 12: Combustor head-end pressure-time profiles of N_2O/HTPB hybrid rocket engine, baseline case (oxidizer mass flow of 0.385 kg/s), and manoeuvring case with spin (7 rps) and augmented oxidizer mass flow (0.975 kg/s), 3 s < t < 10 s

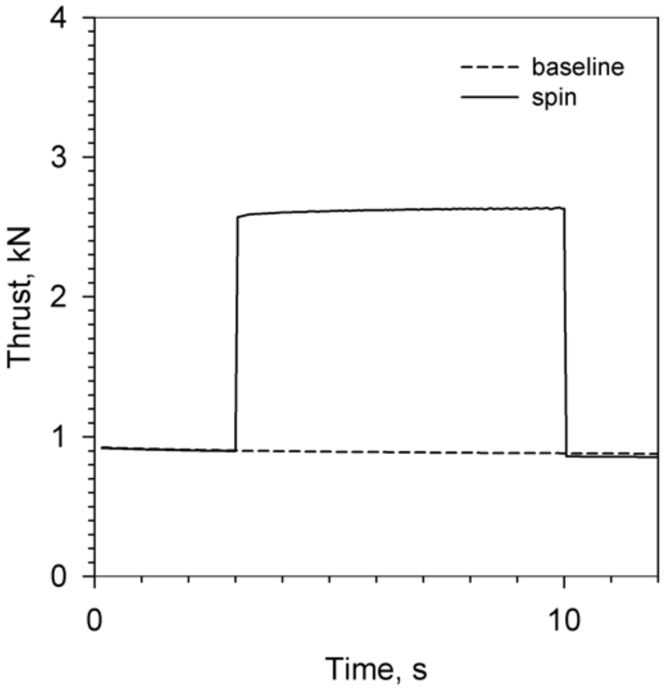

Figure 13: Early part of sea-level thrust-time profiles of N_2O/HTPB hybrid rocket engine, baseline case (oxidizer mass flow of 0.385 kg/s), and manoeuvring case with spin (7 rps) and augmented oxidizer mass flow (0.975 kg/s), 3 s < t < 10 s

One can observe the corresponding sea-level thrust-time profile in Fig. 13. The thrust is augmented to above 150% of the base level during the implementation period. The corresponding stoichiometric length profiles with respect to the HRE's firing time can be found in Fig. 14. Again, from Fig. 14, one can see the need to bump up the oxidizer mass flow during the spin application, to prevent the stoichiometric length from falling too far below 100%.

Given the uncertainty surrounding the predicted effect of acceleration orientation angle ϕ for HREs operating at very low base fuel regression rates, it was decided not to present any simulation results involving forward vehicle acceleration a_ℓ. If the predictive model does have some merit in this domain, one can potentially surmise that the vehicle's forward acceleration a_ℓ can be quite high, and still have significant a_n-induced burning (and corresponding thrust augmentation) under spin. The reader is referred to [4] for further information.

3.3 Possible approaches for spinning an HRE

Applications that may more readily take advantage of the proposed HRE spin technique would be spin-stabilized flight vehicles (complete vehicle under spin) with existing differentially-actuated external aerodynamic control surfaces for controlling the roll of the vehicle (see Fig. 15 for example). This approach, of course, would be more effective in lower atmospheric flight, where the outside air density is more substantial, and with the provision that the vehicle's flight speed is high enough. Alternatively, for lower or upper atmospheric flight at any flight speed, one can employ existing internal hot-nozzle-flow thrust-vector-control (TVC) devices that can induce a roll moment on the vehicle upon command. Mass injection (into the nozzle expansion flow) is a TVC approach that can produce a roll moment, while generating less flow (thrust) losses versus other conventional techniques (like jet vanes placed in the nozzle exit flow) [1]. The reader is referred to [4] for further information.

Other flight vehicle applications may require that only the HRE be rotated, with the forward part of the flight vehicle unrotated. This approach would potentially entail the usage of bearings, slip rings (which allow for electrical signal transmission between the static and rotating vehicle components, in lieu of wireless RF approaches), etc., in accounting for the different motion of the two vehicle components.

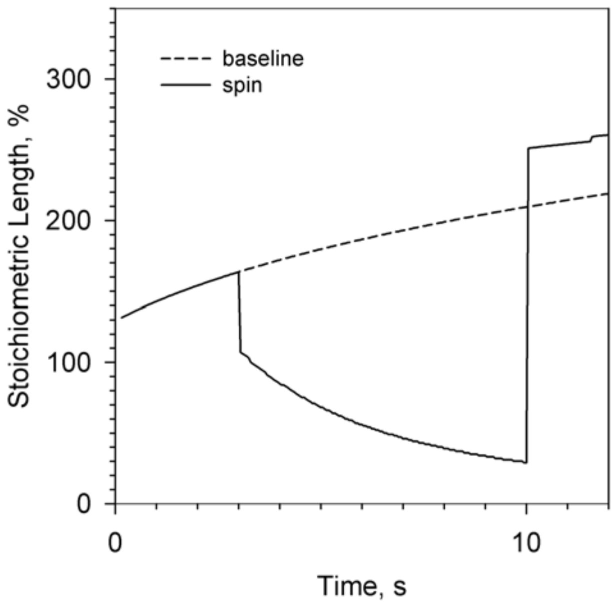

Figure 14: Early part of stoichiometric length-time profiles of N_2O/HTPB hybrid rocket engine, baseline case (oxidizer mass flow of 0.385 kg/s), and manoeuvring case with spin (7 rps) and augmented oxidizer mass flow (0.975 kg/s), 3 s < t < 10 s

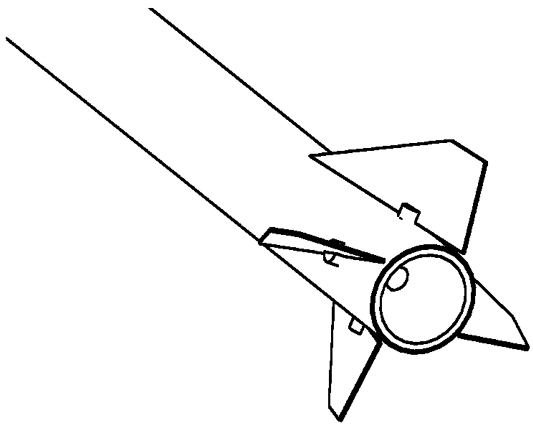

Figure 15: Illustration of roll control approach via differentially-actuated tailfins, to provide engine spin upon command

4. Concluding remarks

With a small sounding rocket as the reference flight vehicle, the use of a hybrid rocket propulsion system that allows for on-command thrust modulation via alternative techniques have been examined in the present performance evaluation study. The thrust modulation technique using head-end oxidizer injection swirl (in conjunction with oxidizer throttling) was demonstrated, an approach that would potentially have the advantage of a greater thrust delivery range (versus throttling alone), in addition to potentially allowing for the use of a single fuel port (versus a less desirable multiple-port arrangement). The alternative thrust modulation technique, through engine spin, is a novel approach that might have some niche application advantages over the more conventional swirl approach.

Getting into more detail, one could undoubtedly argue pro and con as to the complexity and effectiveness of the two approaches. In ultimately choosing between the two thrust modulation choices presented here, or moving in another direction, one would likely need to outline the flight mission requirements for the example flight vehicle in more detail, before proceeding further.

References

[1] Greatrix, D.R. 2012. *Powered Flight – The Engineering of Aerospace Propulsion*, Springer-Verlag London Ltd., London (UK).

[2] Wongyai, P., and D.R. Greatrix. 2014. Regression rate estimation for swirling-flow hybrid rocket engines. In: AIAA/ASME/SAE/ASEE 50th Joint Propulsion Conference, AIAA Paper No. 2014-3750.

[3] Greatrix, D.R. 1996. Internal ballistic model for spinning star-grain motors. *J. Propul. Power*, 12: 612-614.

[4] Bockelt, M.W. 2014. Application of spin and swirl for in-flight thrust modulation of hybrid rocket engines. Diplom-Ingenieur Thesis. Munich University of Applied Sciences, College of Engineering, Department of Mechanical, Automotive and Aeronautical Engineering.